Dynamic Stall Control Investigations on a Full Size Chord Blade Section

by
Wolfgang Geissler, Guido Dietz, Holger Mai, Bernd Junker, DLR-Germany
Thomas Lorkowski, EADS-Germany

Abstract

In the present investigations dynamic stall is controlled by a nose-drooping device, where the 10%-sealed leading edge part of a new supercritical airfoil section drooped down dynamically during the pitching motion of the blade model to alleviate dynamic stall. Both CFD-calculations as well as experiments have been accomplished for these investigations within the scope of the project ADASYS [*] (Adaptive Systems) between the partners: ECD, EADS and DLR. Three different DLR-Institutes were involved in the project: Institute of Aerodynamic and Flow Technology, Institute of Aeroelasticity, both located in Göttingen and Institute of Flight Systems located in Braunschweig, Germany.

Main emphasis in the present discussions is placed on the experimental investigations which have been carried out in the DNW-TWG wind tunnel facility located at DLR-Göttingen. A full size 0.3m chord blade section with 1m span (between the tunnel side walls) has been installed inside the adaptive wall test section of this tunnel. The model made of composite material was suspended in the forced pitch-oscillation test rig of the DLR- Institute of Aeroelasticity.

In addition to the pitching motion of the model about its quarter chord axis, the 10% leading edge part (0.5m span) of the model was oscillated separately from the blade motion in different drooping modes and with phase-variations between blade motion and flap motion. The leading edge deflection has been achieved with piezo-electric actuator devices developed by EADS. The flap/actuator arrangement has been designed as a separate module which could easily be removed from the remainder of the model.

In the present paper experimental results and comparisons with numerical data are discussed for steady as well as unsteady flow cases.

Introduction.

The main objectives of dynamic stall control devices are to keep the benefits of the dynamic stall process, i.e. a considerable increase in maximum lift and simultaneously reduce drag and negative pitching moment peaks as well as negative aerodynamic damping. It is well known, McCroskey, [1] that dynamic stall is characterized by the development, movement and finally shedding of a concentrated vortex, the dynamic stall vortex, which is the origin of lift increase and large drag- and dangerous pitching moment peaks respectively. It is further known that this vortex develops close to the airfoil leading edge.Dynamic stall control devices are therefore assumed to be most efficient if they are located close to the leading edge to influence the dynamic stall vortex at its origin.

Several control devices are known from literature: Fixed leading edge slats for example are able to avoid the dynamic stall vortex completely, [2] but have unacceptable properties on the advancing blade. With an elastically changing leading edge radius, [3] dynamic stall could be influenced very local in the region where the dynamic stall vortex develops. However this device was very fragile and therefore not very suitable for rotor applications. The synthetic jet concept is a further device, [4] which shows benefits not only with respect to steady separation but also for dynamic stall control. Here also the location of the jet(s) namely close to the airfoil leading edge determines whether the device is sufficient or not. Jets can be turned on and off and are therefore suitable for rotating blades. For rotor blade application one has to keep in mind that a device which is effective on the retreating side must not be a disturbance on the advancing side. If portions of the blade are deformed, the deformation has to be done dynamically. This rule makes corresponding devices rather complex.

Within the scope of a MoU (Memorandum of Understanding) between US-Army and DLR a model has been manufactured at Ames Research Center where the 25% leading edge part of the VR12 airfoil could either realize a fixed droop or a variable droop, where in the latter case droop angle and model incidence coincided, [5]. This device is known as the Variable Droop Leading Edge (VDLE) device. Numerical calculations have been carried out before the tests, [6], showing the benefits of the device which have later successfully been verified in the experiments.

The present investigation goes some steps further: the model oscillation about the quarter chord axis is **decoupled** from the motion of the 10%-sealed leading edge flap which is driven separately by an actuator system operated inside the full size chord (0.3m) wind tunnel model.

With this arrangement several additional parameters could be investigated, one of the most important ones is the phase shift between model motion

and flap motion. Due to the decoupling of model motion and dynamic droop the amplitude of the flap motion could also be changed independently from the incidence variation.

The tests have been conducted in the DNW-TWG transonic wind tunnel facility located at DLR-Göttingen, Germany. The adaptive wall test section of the tunnel has been used also during the unsteady tests. In [7] it has been outlined that wind tunnel wall adaptation at the mean incidence of model oscillation shows reduced wall interference effects also during the remainder of the oscillation loop. The experience gained from this pre-test are of considerable benefit also for the present investigations.

The Project ADASYS.

The project ADASYS (Adaptive Systems) is a joint effort between ECD (Eurocopter Deutschland), EADS (European Aeronautic and Space Company) and DLR (German Aerospace Center). The project ADASYS goes a different way compared to usual control efforts to improve the dynamic stall properties of a rotor blade: In a more global perspective **both** the advancing side as well as the retreating side of the rotor blade has been taken into account in the present study, with the aim to improve the flow properties on both sides of the rotor disc. This is achieved by the new design of a supercritical airfoil which has improved properties at transonic flow conditions on the advancing side. To improve the dynamic stall properties on the retreating side a drooping device has been designed and realized in addition.

The project ADASYS is subdivided into different tasks. The present investigations are concerned with **dynamic stall control** on a helicopter rotor blade section by means of a dynamically drooping sealed leading edge flap (nose-drooping device). These investigations have been carried out with the application of both experimental as well as numerical tools. Several steps have been done before to prepare the present work:

1. Design of a supercritical airfoil section DLR-A1510 to optimize the transonic flow properties on the advancing blade. This part has been done by a numerical design procedure developed at DLR, [8],
2. Design of a nose-drooping device (10%-sealed leading edge flap) and CFD-calculations to demonstrate the efficiency of the dynamic drooping flap to favorably control dynamic stall, [9],
3. Dynamic stall measurements as well as transonic measurements in the DNW-TWG wind tunnel on a **rigid** full size blade section with the supercritical A1510 airfoil section as well as corresponding CFD-calculations integrating the RANS-equations for unsteady 2D flow, [7],

4. Present final test with the dynamically nose-drooping device.

The present most complex part of the project has two main objectives:
1. show that a dynamically drooping leading edge flap integrated inside an oscillating blade section is feasible and works sufficiently,
2. show that previously observed benefits of the nose-drooping concept by CFD-calculations are realistic and can be verified in experiments.

Model with Nose-Droop Control.

The wind tunnel model with nose-droop device has a span of 1m and fits between the side-walls of the 1m × 1m adaptive wall test section of the DNW-TWG wind tunnel, **Fig.1**. The model chord is 0.3m which is assumed as full scale for a medium size helicopter rotor blade. The model has been oscillated in pitching mode (simulation of cyclic pitch) about the quarter chord axis at constant free stream conditions. The sealed leading edge flap with 0.5m span-wise extension symmetrically about mid span oscillated independently from the model motion about the 10% chord flap hinge.

The model was manufactured from composite material (CFK) to keep the weight to a minimum and the stiffness to a maximum. The movable leading edge flap part including its instrumentation was designed as a separate module which can completely be removed from the remainder of the model. **Fig. 2** shows the nose-droop module including the actuator system before assembling. The advantage of the present design is the possibility to remove the complete unit from the model for maintenance. A failure of one of the piezo-stacks during the wind tunnel tests made it necessary to remove the unit which could then be repaired outside the test section without loosing much of expensive wind tunnel time.

Fig.1: Model in DNW-TWG test section
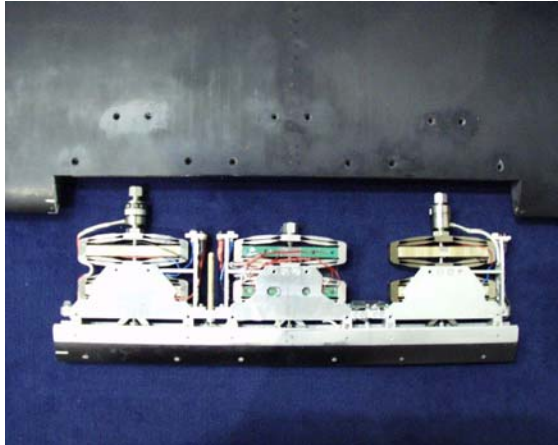
Fig.2: Nose-Droop Actuator before assembling

Fig.2 further shows that the nose-droop device is subdivided into three aluminum frames each equipped with two coupled actuator units. A mechanical gear transfers the longitudinal displacements of the piezo-stacks into a rotational motion of the leading edge flap. Details of the construction are reported in [10].

The piezo-electric actuators evolved from parallel investigations on a full scale rotor and proved also outstanding performance under harsh vibratory and centrifugal conditions, [13].

Fig.3 shows a side view of the movable leading edge device installed in the model. A crucial part of the construction is the transient between the moving leading edge surface and the fixed remainder of the model surface.

The objectives here are:
- avoid flow from the pressure side to the suction side through gaps,
- get smooth transients also during nose-droop motion,
- avoid forward facing steps which could affect the rather thin boundary-layer in that region.

The first and second objective could only be reached approximately. The third objective has been sufficiently fulfilled on the upper surface (see Fig.3).

Fig.3: Movable Leading Edge, Side-View

On the lower surface the gap has been kept as small as possible, but here a discontinuity is not as critical as it is on the upper surface.

Bolts fitting into holes at both span-wise edges of the flap unit (see Fig.3) are used for some test cases to definitely hold the flap unit in a zero droop position.

Instrumentation.

The model was equipped with sets of different sensors:

- Upper surface: 29 miniature pressure sensors of differential type (Kulite XCS-093 or LQ-164),
- Lower surface: 17 pressure sensors of differential type (Kulite XCS-093),
- 2 accelerometers (PCB 352C22),
- 3 Hall-sensors to measure the rotation angle of the flap versus the model (MICRO-NAS-805),
- 2 load cells on the outer actuator-units.

The pressure sensors have been arranged along mid-chord of the model; a total of eleven sensors are installed in the flap unit. The reference sides of the pressure sensors have been collected into some few flexible reference tubes which were led out of the model through the model axis. This latter arrangement caused a problem during the tests: ten sensors along the model lower surface which were gathered into one reference tube showed wrong reference pressures: It is assumed that during model assembly the reference tube has been squeezed together such that it was almost closed .

It will be shown in a later section how these pressure sensors can still be used with the application of a simple correction procedure.

The three Hall-sensors have been installed in each of the three actuator compartments (see Fig. 2). HALL-2 is installed close to the flap mid-section and is therefore close to the pressure measuring section.

Permanent magnets were fixed on the nose-droop device, the sensors have been fixed to the blade structure. These sensors are very small and have nonlinear characteristics. Problems occur if the bearings of the moving part have some free play which may have been grown during the test period. A distinction between the pure flap rotation and the movement due to bearing free play is not possible. These effects seem to be of some importance in the present test.

The positioning of the nose-droop device was performed by a PID-controller which used the mean value of the three HALL-sensor signals as input taking into account their nonlinear characteristics.

Preparation of Numerical Calculations.

For numerical calculations with the RANS-code, [11] the definition of the deflection history of the dynamic leading edge flap has to be specified. In [9] calculations have been discussed with a 10° droop flap. In the present tests it was found that the goal to operate the flap with 10° flap amplitude was not feasible. Due to the aerodynamic pitch-up moment acting on the flap the actuators achieved only about 6° maximum deflection amplitude at M=0.31 which was further reduced with growing air loads at increasing Mach number.

Fig.4 shows the droop history for 6° flap amplitude represented by 21 single shapes.

The time variation of the single shapes has been arranged as a $\sin^2$-wave (see section "Unsteady results"). In both calculation and experiment a phase shift of the flap motion compared to the model motion can be realized: zero phase assumes that maximum droop and maximum incidence coincide. Positive phase shift means a shift towards the up-stroke, a negative phase means a shift towards the down-stroke of the model. Positive phase shift (phase lead of the flap) is the more meaningful case. Emphasis is therefore placed on phase lead.

A further parameter to be specified is the extend of the drooping motion in comparison to one period of model motion. Two cases have been specified and realized both numerically and experimental: DROOP1 is extended over half the oscillation period of the model (rigid airfoil for the remainder of the period), DROOP2 is extended over the full period.
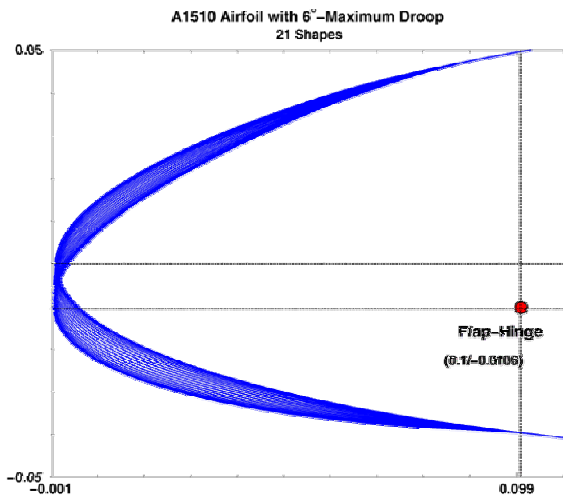
Fig.4: Shape variation at airfoil leading edge with 21 shapes from basis A1510 airfoil to 6° maximum droop.

Correction Procedure of Unsteady Pressures.

It has been mentioned above that the signals of 10 pressure sensors on the lower surface of the model were not easily to be evaluated due to a squeezed reference tube. **Fig.5** shows as an example instantaneous pressure distributions at 10° up-stroke motion for the $\alpha=10^o\pm10^o$ deep dynamic stall case. Displayed are results from the present test campaign compared with corresponding results from the preparation test on a rigid A1510 model in 2002, [7] with the same model size, wind-tunnel test section and wall adaptation. It was observed during the steady tests that the reference pressure did not change while recording a measuring point, thus, the reference tube was sufficiently closed. Therefore, reference pressures have been determined from the 2002 test campaign at 10° up-stroke for the 10 Kulites under consideration (Fig.5) and used as corrections for the entire oscillation cycle.
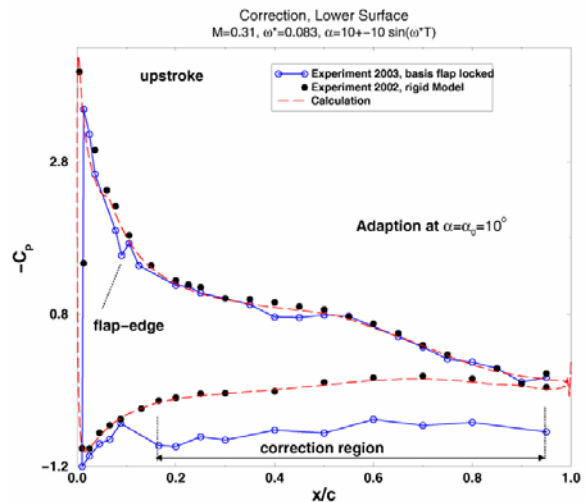
Fig.5: Reference Pressure Correction

For the drooping cases it has been observed from numerical results that almost no differences occur on the lower surface compared to the basis case without droop. The correction from the basis-case has therefore also been used for the drooping cases.

Results.

The following discussion of results is subdivided into a discussion of steady measured and calculated pressures at various incidences and with/without droop, followed by the investigation of unsteady force and moment hysteresis loops for the two cases: Light Dynamic Stall and Deep Dynamic Stall both at M=0.31, Re=$1.15\cdot10^6$, Su_0=110.4K/T_0=0.37. Comparisons of measured data with simulation results are discussed then and finally some few pressure distributions for transonic flow are presented as well.

Steady Results at Mach number M=0.31.

Fig.6, Basis A1510 airfoil and **Fig.7**, airfoil with constant 10° droop show steady pressure distributions at various incidences at M=0.31. Solid lines are calculations, symbols in the same color indicate

the corresponding experimental data (measured pressures on the lower surface have been omitted here).

In the basis case (Fig.6) the flap has been locked by means of the sliding bolts fitting into the holes of the flap-unit side edges (see Fig.3). This arrangement guaranteed a fixed position of the flap without deflection. In most test cases the flap was hold in a fixed position by means of the actuator forces alone. It will be shown that during model motion the flap could not be kept in a fixed position: either aerodynamic forces and/or inertia forces are responsible for this behavior.
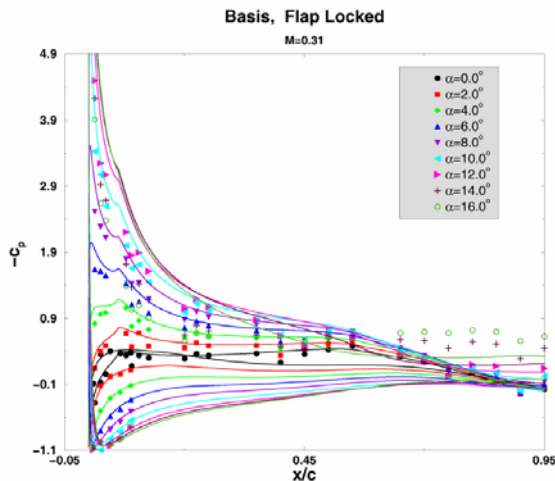
Fig.6: Calculated and measured static pressure distributions for various incidences, Basis case (no droop)
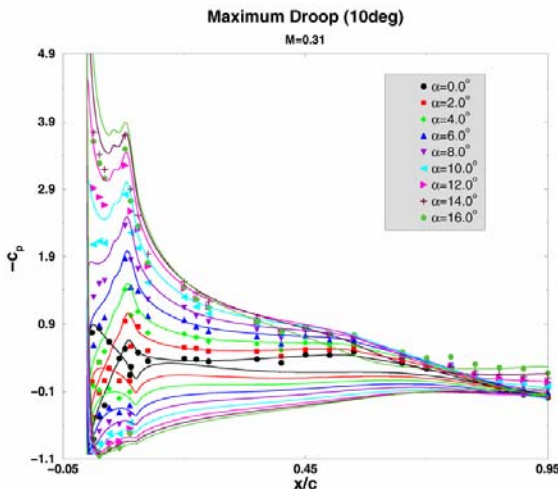
Fig.7: Calculated and measured static pressure distributions for various incidences, 10°-Droop.

With increasing incidence the leading edge pressure peak is developing and finally leads to flow separation at the trailing edge between about $\alpha=12^o$ and 14°. The calculations follow these trends however show some less sensitivity with respect to separation. It has been discussed already in [7] that the

turbulence model, here the Spalart/Allmaras model may be responsible for this behavior.

In the droop case, Fig.7, the pressure minimum is shifted downstream at low incidences until a leading edge peak is developing at higher incidences. Trailing edge separation in this case is almost avoided in the incidence regime displayed. The correspondence between calculation and experiment is very good in the low incidence regime, some deviations occur on the flap at increasing incidences which must be attributed to either some flow through the small gap between flap and model (Fig.3) and/or some discontinuities due to a non-smooth transient between flap and model.

These observations are also found later in the unsteady pressure distributions of the dynamic stall flow cases and can also be found in the hysteresis loops of forces and moment.

Unsteady flow cases.

A large amount of different flow cases have been measured during the present test campaign. For all pressure and HALL-sensor data 128 points per period of blade motion have been taken over a total of 160 periods. Only a few typical results have been selected for the present paper:

- Light dynamic stall case: $\alpha=10^o\pm5^o$
- Deep dynamic stall case: $\alpha =10^o\pm10^o$

with different oscillation frequencies of the blade motion at M=0.31.

Two instantaneous droop variations have been applied:

- DROOP1 (droop over half period, rigid airfoil for the remainder of the period),
- DROOP2 (droop over full period).

The phase angle between blade motion and flap motion is varied to study its effect with respect to optimum flow characteristics. Of main concern is a positive phase shift, i.e. a shift towards the model up-stroke motion (phase-lead of the flap).
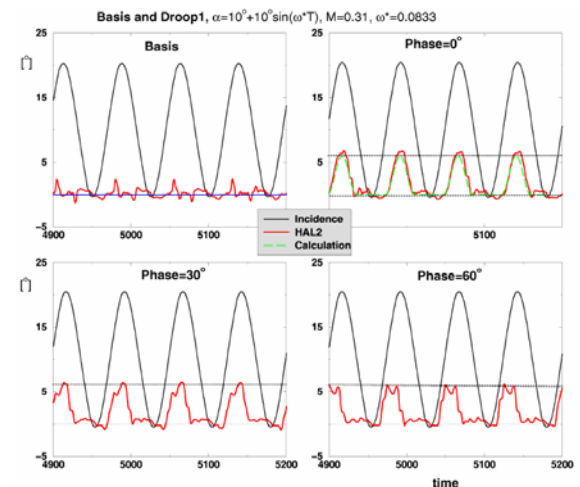
Fig.8: DROOP1, incidence variation, flap deflection (HALL-2, at mid-section) for basis case (no droop) and with dynamic droop, different phases.

Fig.8 shows incidence variations versus time and dynamic flap deflections as measured with the HALL-sensor 2 at mid-chord for

a) Basis case (no droop)
b) Dynamic DROOP1 over half period for phase-angles: $0^o, 30^o, 60^o$.

The graph for zero phase angle includes in addition the corresponding numerical signal as a $\sin^2$-wave.

Basis case means here different to the steady arrangement discussed before that the flap was forced to stay in a fixed (zero) position by electrical forces of the actuator unit. As can be seen in Fig.8 this goal has not been achieved: Close to the end of up-stroke a positive deflection (pitch-down) and close to the end of down-stroke a negative deflection (pitch-up) is observed. Looking into flow details these effects are in coincidence with the occurrence and disappearing of unsteady separation effects (dynamic stall vortex shedding) where severe short-time aerodynamic force and moment peaks over-strain the holding actuator forces. Furthermore, at the maximum incidence a negative deflection (pitch-up) is observed due to the inertial moment of the flap.

In the cases with dynamic droop the HALL-sensor signals show some scatter at the time-instants where unsteady forces and moments are large.

Very similar results have been achieved for the DROOP2 case, displayed in **Fig.9**. The dynamic droop is now distributed over the whole oscillation period of the blade model. The plot for phase-angle equal zero includes again the corresponding numerical results. The different HALL-sensor signals show again remarkable deviations from the ideal $\sin^2$-wave representing the numerical case. The kinks in the curves clearly indicate that the problem occurs during up-stroke close to dynamic stall onset.
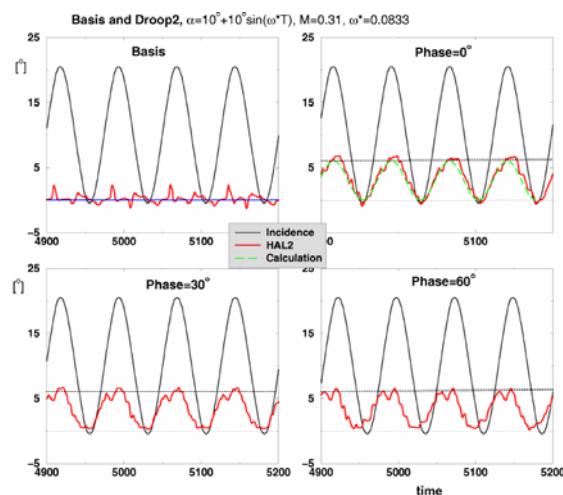
Fig.9: DROOP2, incidence variation, flap deflection (HALL-2, at mid-section) for basis case (no droop) and with dynamic droop, different phases.

The incidence and flap deflection time histories displayed in Figs. 8 and 9 represent the deep dy-

namic stall cases. Corresponding results for the light dynamic stall case (not displayed) show a similar behavior with less wiggles of the HALL-sensor signal due to less severe stall events.

Measured force- and moment- hysteresis loops,
a) Deep Dynamic Stall case.

With a mean incidence of 10° and 10° amplitude of the blade pitching motion the incidence variation covers the regime between 0° and 20°. This incidence variation is assumed as a deep dynamic stall flow case characterized by development and shedding of a strong dynamic stall vortex. Vortex shedding causes steep increases of drag and pitching moment peaks.

Fig. 10 shows first of all lift-, pressure drag- and pitching moment hysteresis loops for:

- Basis case (no droop),
- DROOP1 flap deflection with different positive phase-angles.

These results are phase-locked averages of all measured 160 periods.

The differences between the basis case and the drooping case are indicated in the three plots:

- the maximum lift peak is shifted slightly towards higher incidence, the maximum lift is not changed,
- the maximum pressure drag has been reduced in the present case by 18%,
- the negative pitching moment peak is reduced as well by 20%.
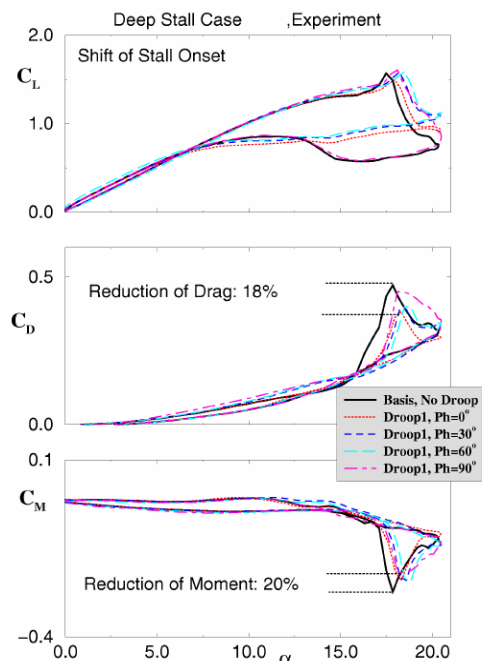
Fig.10: Lift-, drag- and pitching moment loops for deep dynamic stall case, DROOP1-flap deflection.

These improvements have been obtained at small phase angles of about 0° to 30°. At higher positive phase shifts the improvements are reduced.

Very similar results are obtained with the second flap deflection history, i.e. DROOP2 which is extended over the whole period of blade movement, **Fig.11**.
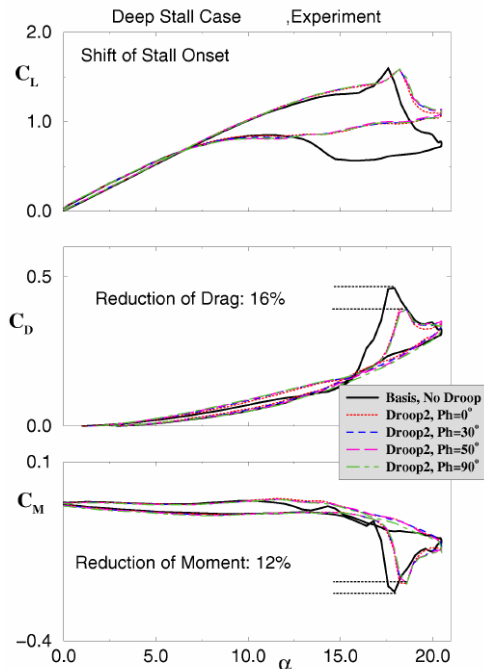
Fig.11: Lift-, pressure drag- and pitching moment loops for deep dynamic stall case, DROOP2-flap deflection.

Reductions of maximum drag and minimum pitching moment are smaller compared with the DROOP1 case, the effect of phase variation has only small influence on the peak values.
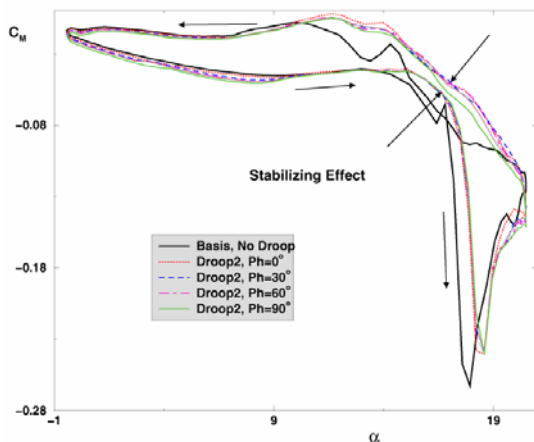
Fig.12: Details of moment hysteresis loop for DROOP2.

Fig. 12 is focusing on another important phenomenon which could favorably be influenced by phase

shifting between blade and flap motion. It is well known that the area between moment loops is an indicator of aerodynamic damping. The sense of traversing the loops determines whether the system is damped (counter clockwise) or un-damped (clockwise). Fig.12 shows that for the basis, no droop case an overlapping of up-stroke and down-stroke curves occurs which is completely avoided with flap motion. Again the phase angle plays an important role: Between 0° and 60° curves are separate and aerodynamic damping is achieved for the whole loop. At higher phase-angles (here at 90°) the trend is reversed, the gap between up-stroke and down-stroke parts of the cycle is reduced.

These results are very remarkable because it shows that with the present control device not only peak values of drag and pitching moment could be reduced by keeping maximum lift unchanged, but also the aerodynamic damping characteristics and hence the aeroelastic properties of the system could be improved by the nose-droop device.

Similar results have also been observed previously in nose-drooping tests at Ames Research Center, [5], with a larger (25%-chord) leading edge flap drooping with much larger deflection angles:

$$\alpha = \delta_{droop}$$

Now it is clearly demonstrated that the phase relationship between the two motions plays an important role and optimization of benefits is possible with respect to phase angle variation.
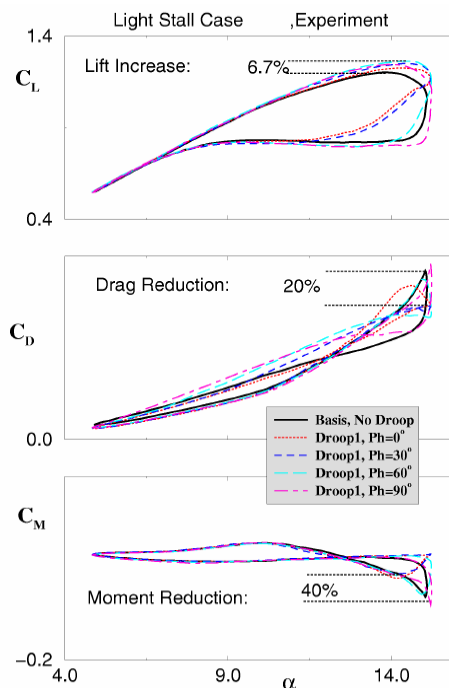
Fig.13: Lift-, pressure drag- and pitching moment loops for light dynamic stall case, DROOP1-flap deflection.

b) Light Dynamic Stall Case.

Fig.13 shows the corresponding force- and moment loops for the light dynamic stall case: $\alpha=10^o\pm5^o$ again at M=0.31 and a reduced frequency of 0.1 referred to airfoil chord.

Now in addition to severe improvements of drag and moment peaks the maximum lift is even increased slightly due to the drooping motion. Again the phase angle plays an important role as has been pointed out for the deep stall cases: no it can be observed that optimum results are obtained at about 30° phase shift.

It must be kept in mind that these remarkable results have been achieved with a small size flap of only 10% chord with maximum deflection angles of about 6°. It is quite obvious that larger effects are possible with either a larger flap size and/or increased flap deflection angles.

Fig. 14 finally displays the hysteresis loops for the light stall case and DROOP2 flap deflection.

All features discussed already for the DROOP1 variation are detected also in the DROOP2 case. Optimum reductions of drag and moment peaks are obtained at slightly higher phase shifts up to 60°.

It should be mentioned here that a light dynamic stall case is much more sensitive with respect to its control compared to the deep dynamic stall cases displayed in Figs. 10 to 12. In the latter cases the dynamic stall vortex could not be avoided but has been influenced in a favorable way.
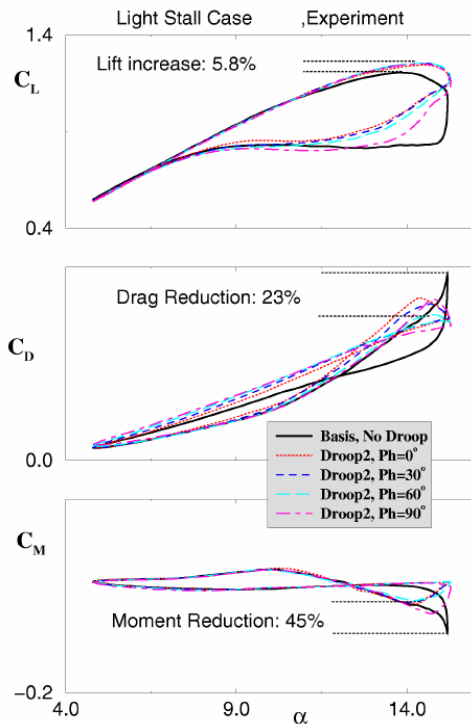
Fig.14: Lift-, pressure drag- and pitching moment loops for light dynamic stall case, DROOP2-flap deflection.

Numerical calculations and comparisons with experiment.

In addition to the experiments numerical calculations have been carried out and compared with the measured data. **Fig.15** shows first of all pure numerical results of unsteady force- and moment hysteresis loops. Displayed are results (DROOP2) for the basis airfoil and the drooping airfoil with zero and $\pm45^o$ phase shift. The trends observed in the experimental data are also found in the calculations:
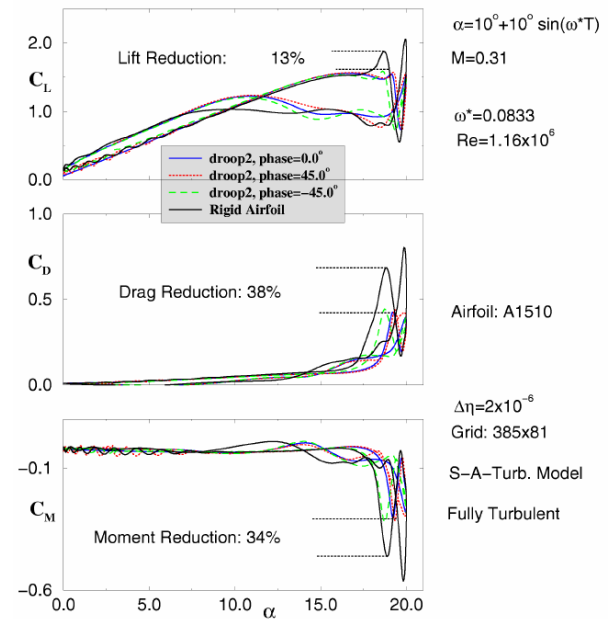
Fig.15: Numerical results for the Deep Dynamic Stall case.

With positive phase shift the maximum lift is shifted to higher incidences, the maximum drag and minimum pitching moment peaks are considerably reduced. However the reductions are larger compared to experiments. The lift shows a lack of extra peak caused by the dynamic stall vortex. This may be explained as follows: Due to a gap between flap and airfoil the flap efficiency has been reduced in the experiment. The dynamic stall vortex is still existent and drag and moment peak reduction is only moderate (see Figs.7 and 11).

It has already been discussed in [7] that a secondary force- and moment peak is observed in the present 2D-calculations once the primary vortex, i.e. the dynamic stall vortex is shedding into the wake. This secondary effect can not be observed in the experiments. It is assumed that the dynamic stall vortex is with very good approximation a two-dimensional event with a vortex generator orientated parallel to the model leading edge. A 2D-representation of this vortex is hence a valid assumption. The following secondary vortex is represented as a 2D-structure as well which does not match the reality: Once the

dynamic stall vortex is shedding a very complex unsteady separated 3D-flow occurs on the model upper surface with strong pressure fluctuations and therefore also fluctuations of forces and moment from period to period. Secondary peaks due to vortex development and shedding are still visible in the experimental data: However their effects are rather small. In future investigations it is of crucial importance to get detailed information of the unsteady flow fields in the unsteady separated upper surface flow region. This information can be obtained by optical measuring techniques like the Particle Image Velocimetry (PIV).

It can further be observed from Fig.15 that a shift of the phase into the negative direction, i.e. towards the down-stroke of the model motion leads still to
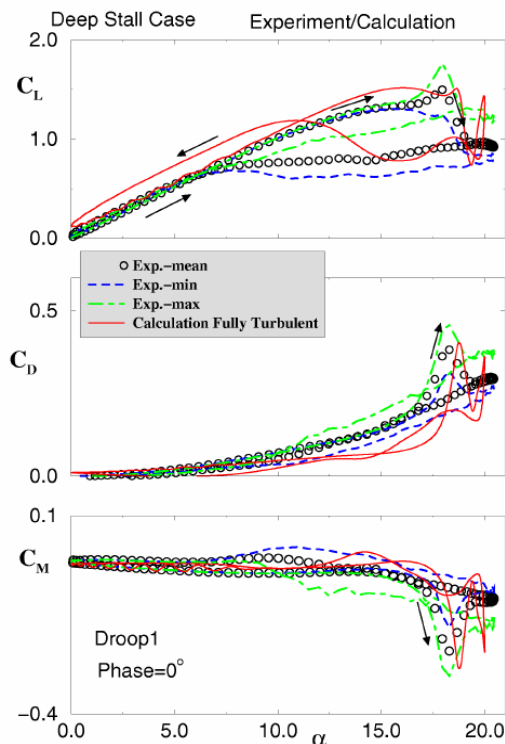
Fig.16: Deep Dynamic Stall, Comparison of calculation and Experiment.

improvements of the peak maximum but stall onset is occurring earlier in the loop, a behavior which can also be found in the data.

Fig. 16 shows numerical as well as experimental results for the Deep Dynamic Stall case with DROOP1 (Phase=0°). For the experimental data three different curves have been included:

1) Mean values obtained by phase-locked averaging over 160 periods (indicated by circles),
2) Minimum values (blue dashed),
3) Maximum values (green dashed).

One can observe that all three curves are identical in regions without separation. Once dynamic stall onset occurs all three curves start to deviate from each other considerably.

Numerical results (red solid curves) are also included in the graphs. The Spalart/Allmaras turbulence model combined with the option fully-turbulent flow has been utilized. Very good coincidence between calculation and experiment is observed at low incidences and up to ~16° upstroke where dynamic stall onset occurs with the characteristic
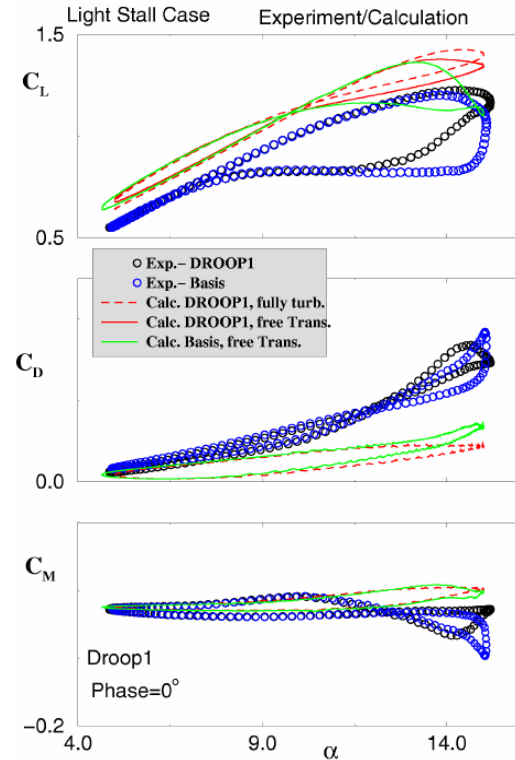
Fig.17: Light Dynamic Stall, Comparison of calculation and Experiment.

extra peak in lift. The correspondence between calculation and experiment is very good.

Beyond dynamic stall onset the previously discussed secondary peaks occur in the calculation which cannot be observed in the data, although it is obvious that the three curves from measurements (mean, min, max) cover a rather large area representing the whole time series of the experimental data.

During down-stroke the reattachment process is starting earlier in the calculation until correspondence is achieved again during the lower incidence portion of the down-stroke.

Fig. 17 finally shows the case of Light Dynamic Stall with again both numerical and experimental data. This case is characterized by strong sensitivities in both numerical and experimental data. The sensitivity in the numerical results is mainly caused by the turbulence modeling and in addition by the effects of transition. Therefore the basis case and drooping case are calculated with the transition option "free transition" utilizing Michel's criterion of transition onset and the Chen-Tyson function to model the transition region, [12]. In the experiments Basis and DROOP1 cases are included. It is

seen that also in the low incidence region of the lift hysteresis loops a considerable parallel shift of the calculation towards higher values is achieved. The explanation of this behavior may be the same as has already been discussed for the steady results (see Fig.7): Over the leading edge flap does occur a lift loss probably due to flow through the gap between flap and main part of the airfoil. This lift loss keeps the hysteresis curves on a slightly lower level. Comparing the lift distribution with the one obtained in the 2002 campaign with the rigid airfoil the coincidence with the numerical data is almost perfect (not indicated in Fig.17).

Transonic flow.

To investigate the flow about the drooping airfoil in transonic flow, i.e. at M=0.73 (design Mach number for the A1510 airfoil) some steady as well as unsteady tests have been carried out also in this high speed flow regime. In the following discussion
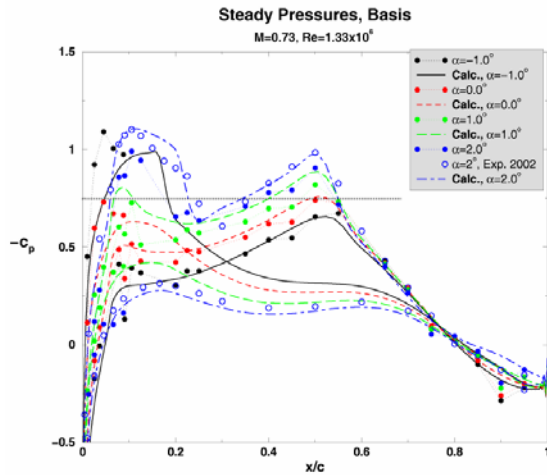
Fig.18: Steady pressures at transonic flow, basis airfoil.
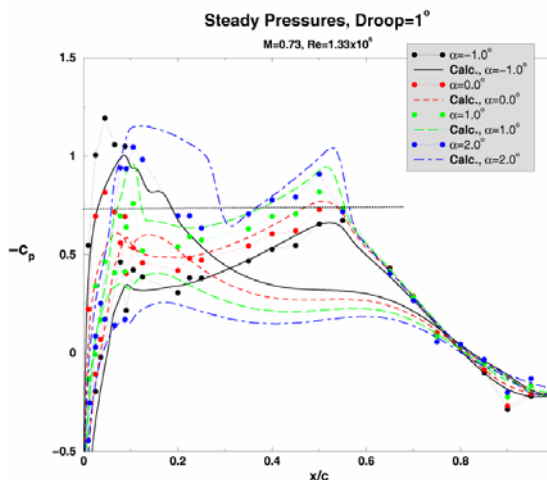
Fig.19: Steady pressures at transonic flow, airfoil with 1°-droop

some characteristic steady results have been depicted to investigate the effects on the airfoil without and with droop:

Fig.18 displays pressure distributions about the basis airfoil without mechanical locking. Typical deviations occur between calculations and experimental data on the flap upper surface: As mentioned before the pressures are strongly reduced close to the transient between flap and the main airfoil. The plot also includes a result from the 2002 campaign, [7] with the rigid airfoil model (2° incidence). The calculations match the measured data fairly well in this case. For the airfoil with static 1°-droop, **Fig.19,** similar strong deviations occur on the flap upper surface. The effects may be caused by the special model arrangement (gap-effect), the output of the HALL-sensors for this case show a good representation of the 1°-droop.

In the unsteady cases the mean incidence of 1.5^o and 0.5^o amplitude has been realized. The HALL-sensor data show that the actuator device was able to realize this incidence variation also under transonic flow conditions.

Conclusions and Outlook.

Dynamic stall control by a dynamically operating nose-droop device has been investigated in the 1m × 1m adaptive-wall test section of the DNW-TWG wind tunnel facility at DLR Göttingen, Germany within the scope of the project ADASYS (Adaptive Systems). The full size chord (0.3m) blade section was oscillated about its quarter chord axis by means of the forced pitch-oscillation test rig of the DLR-Institute of Aeroelasticity. The 10%-leading edge part of the model was oscillating in addition, separately but synchronized about the flap hinge. The sealed flap was operated by a piezo-electric actuator device with a maximum dynamic flap deflection of 6° at M=0.31. The frequencies of model and flap oscillations were in coincidence. The phase between both the model and the flap motion has been varied and found as an important parameter to optimize dynamic-stall control by the present nose-droop device.

In addition to wind tunnel tests numerical calculations have been performed in parallel investigating the same set of parameters. The main objectives of the project ADASYS have clearly been reached:

- The feasibility of the complex test with two different and independent oscillatory motions on the model has been demonstrated,
- The main objectives of dynamic stall control, i.e. the reduction of drag and moment peaks without lift loss has been achieved,
- Results of numerical calculations show very similar trends as experimental data. Differences still occur due to deficiencies in turbulence and transition modeling.

Some deficiencies of the model have also been observed during these investigations:

- the model manufacturing has to be improved to avoid malfunction of sensors,
- the transient between flap and main airfoil must carefully be modeled to avoid flow through gaps and from that reductions of flap efficiency,
- the actuator forces have limits to sufficiently take care of strong peaks in aerodynamic loadings as well as realizing sufficient droop amplitudes.

The tests have shown that a continuation of the present work is highly recommended. The variation of the phase angle between blade motion and flap motion should play a key role for further investigations: A systematic phase variation has already shown its favorable effects with respect to an optimum control.

References.

[1] McCroskey,W.J., "The Phenomenon of Dynamic Stall", NASA TM-81264, March 1981.

[2] Carr,L.W., McAlister,K.W., "The Effect of a Leading Edge Slat on Dynamic Stall of an oscillating Airfoil", AIAA Paper 83-2533, Oct. 1983.

[3] Chandrasekhara,M.S., Wilder,M.C., Carr,L.W.. "Compressible Dynamic Stall Control using a Shape Adaptive Airfoil", AIAA Paper 99-6650, Jan.1999.

[4] Hassan,A.A., Nagib,H., Wygnanski,I., "Oscillatory Jets-Benefits and Numerical Modeling Issues", Paper 58th AHS-Forum, Montreal, Canada, June 11-13, 2002.

[5]Martin,P.B., McAlister,K.W., Chandrasekhara,M.S., Geissler,W., "Dynamic Stall Measurements and Computations for a VR12 Airfoil with a Variable Droop Leading Edge", Paper on 59th AHS-Annual Forum, Phoenix , AZ, May 6-8, 2003.

[6] Geissler,W., Trenker,M., "Numerical Investigation of Dynamic Stall Control by a Nose-Drooping Device", AHS-Aerodynamics and Acoustics Technical Specialists Meeting, San Francisco, CA, January 23-25, 2002.

[7] Geissler,W., Dietz,G., Mai,H., "Dynamic Stall on a Supercritical Airfoil", 29th European Rotorcraft Forum, 16-18 Sept., 2003, Friedrichshafen Germany, Paper Nr.51.

[8] Geissler,W., Trenker,M., Sobieczky,H., "Active Dynamic Stall Control Studies on Rotor Blades", Research and Technology Agency, Spring 2000 Symposium on Active Control Technology, Braunschweig, Germany, 8-12 May, 2000.

[9] Geissler,W., Sobieczky,H., Trenker,M., "New Rotor Airfoil Design Procedure for Unsteady Flow Control", 26th European Rotorcraft Forum, The Hague, The Netherlands, Sept.26-29, 2000, Paper Nr.31.

[10] Lorkowski,T., "Piezoelektrische Hybridaktuatoren für eine dynamische Profilvariation als Hochauftriebshilfe an Helikopterrotoren", Fortschritt-Berichte VDI, Reihe 12, Nr.451, (in German), June, 2000.

[11] Geissler,W., "Instationäres Navier-Stokes Verfahren für beschleunigt bewegte Profile mit Ablösung (Unsteady Navier-Stokes Code for Accelerated Moving Airfoils including Separation)" in German, DLR-FB 92-03, 1992.

[12] Geissler,W., Ruiz-Calavera,L.P., "Transition and Turbulence Modeling for Dynamic Stall and Buffet",4th International Symposium on Engineering Turbulence Modeling and Measurements, Frantour&CCAS, Porticcio Ajaccio,Corsica, France, May 24-26, 1999.

[13] Enenkl,B., Klöppel,V., Jänker,P., "Full Scale Rotor with Piezoelectric Actuated Blade Flaps", 29th European Rotorcraft Forum, 17-19 Sept., 2002, Bristol UK, Paper Nr. 89.